HHS Public Access

Author manuscript

Pediatr Res. Author manuscript; available in PMC 2016 March 30.

Published in final edited form as:

Pediatr Res. 2012 April ; 71(4 Pt 1): 338–344. doi:10.1038/pr.2011.74.

The perinatal transition of the circulating metabolome in a nonhuman primate

Andrew C. Beckstrom[1], **Pattaraporn Tanya**[1], **Elizabeth M. Humston**[2], **Laura R. Snyder**[3], **Robert E. Synovec**[2], and **Sandra E. Juul**[1]

[1]Department of Pediatrics, University of Washington, Seattle, Washington

[2]Department of Chemistry, University of Washington, Seattle, Washington

[3]Department of Pathology, University of Washington, Seattle, Washington

Abstract

INTRODUCTION—The fetal-to-neonatal transition is one of the most complex processes in biological existence; much is unknown about this transition on the molecular and biochemical level. Based on growing metabolomics literature, we hypothesize that metabolomic analysis will reveal the key biochemical intermediates that change during the birth transition.

RESULTS—Using two-dimensional gas chromatography coupled with time-of-flight mass spectrometry (GC × GC–TOFMS), we identified 100 metabolites that changed during this transition. Of these 100 metabolites, 23 demonstrated significant change during the first 72 h. Of note, four intermediates of the tricarboxylic acid (TCA) cycle were identified (α-ketoglutaric acid, fumaric acid, malic acid, and succinyl-CoA), demonstrating a consistent rate of rise during the study. This may signify the transition of the neonate from a hypoxic *in utero* environment to an oxygen-rich environment. Important signaling molecules were also identified, including *myo*-inositol and glutamic acid.

DISCUSSION—GC × GC–TOFMS was able to identify important metabolites associated with metabolism and signaling. These data can be used as a baseline for normal birth transition, which may aid in future perinatal research investigations.

METHODS—Late-preterm *Macaca nemestrina* were delivered by hysterotomy, with plasma drawn from the cord blood and after birth at eight additional time points to 72 h of age.

INTRODUCTION

The fetal-to-neonatal transition is one of the most complex physiologic, molecular, and biochemical processes in biologic existence. Although the physiology of the birth transition has been well characterized in recent decades, intricacies behind this change remain a mystery. There is a profound change as the fetus moves from a hypoxic intrauterine environment, with codependence on the placenta and its own body, to an oxygen-replete environment in which the baby must function with complete independence.

Correspondence: Sandra E. Juul (sjuul@uw.edu).

The birth process includes the abrupt disconnection from the placenta upon cord clamping, changing the low systemic pressure system to a high-pressure system, which redirects blood flow away from the placenta and toward the newly expanded lungs (1). A body that was once dependent on multiple shunts, such as the ductus arteriosus, becomes a closed-loop circulatory circuit (2). This is aided by the marked decrease in pulmonary vascular resistance that occurs with the alveolar-distending first breath. Some of the molecular bases for these changes have been investigated, including the pulmonary vasodilatory effects of oxygen (3), the rapid clearance of alveolar fluid by amiloride-sensitive sodium channels (4), and the oxidative stress seen following the transition from a hypoxic to an oxygen-rich environment (5,6).

Our understanding of the metabolic changes during the perinatal transition is limited to single pathways, such as changes of glucose levels following birth, and results from a limited number of studies investigating the birth process using a sheep model (7). Recent developments in chemical analysis technology that are being used elsewhere in neonatal research (8,9) can help us understand how the birth transition occurs on a biochemical level. Many metabolites are involved in multiple cycles throughout the body. For example, glutamic acid is crucial in neuronal signaling, the urea cycle, and aerobic metabolism. Therefore, analyzing the complete biochemical profile associated with various stages of the birth transition will help increase our understanding of processes at the cellular level.

Metabolomics is the study of small-molecule metabolites (such as metabolic intermediates, signaling molecules, and secondary metabolites) found within biological samples (10,11). Knowledge of these metabolites can be used to gain a better understanding of the metabolic pathways under investigation. Multiple instrumental platforms are available for analyzing metabolites. These include ultraviolet–visible, infrared, and Fourier transform-infrared spectroscopies (12); nuclear magnetic resonance (13,14); capillary electrophoresis (15); and liquid or gas chromatography (GC) combined with mass spectrometry (MS; refs. 16,17). The most common platforms used in previous metabolomic studies are nuclear magnetic resonance, liquid chromatography–MS, and GC–MS. No single instrumental platform currently available satisfies all the criteria: lack of bias, unambiguous identification, detection sensitivity, reliability, speed, cost, and ease of downstream analysis. To address many of the deficiencies of the commonly used technologies, researchers have recently begun to apply third-order hyphenated instrumentation to metabolomics studies. In particular, comprehensive two-dimensional GC coupled to time-of-flight MS (GC × GC–TOFMS) has emerged as a powerful chemical analysis tool for the study of complex samples, such as those found in metabolomics investigations (18–23).

We recently reported the use of GC × GC–TOFMS in conjunction with innovative chemometric data analysis tools to characterize the metabolic effects of birth asphyxia in a nonhuman primate model (24). We now describe the biochemical changes that occur as nonhuman primates transition to extrauterine life in the absence of experimental asphyxia. Using GC × GC–TOFMS, we examined the plasma metabolome of six primates before and in the days following delivery. We identify key metabolites that change during this perinatal period in a nonhuman primate delivered by hysterotomy. To our knowledge, this is the first

report of the metabolomic changes associated with the fetal transition to becoming a neonate.

RESULTS

Primate Characteristics

Six primates were included in this study, each delivered at a gestation comparable to a 36-wk human gestation. Table 1 illustrates the characteristics of the six primates immediately following birth. Each primate was similar in size by birth weight. The Apgar scores at 1, 5, and 10 min show that the primates responded favorably to delivery and initial resuscitation by the team of neonatologists. Vital signs were measured at 1- to 3-h intervals over the first 12 h. The 0-min pH and partial CO_2 from the primate cord blood demonstrate a physiologically stable intrauterine environment at the end of each pregnancy. The 3-hour pH and partial CO_2 demonstrate the transition of each primate from the intrauterine to extrauterine environment. Each primate was managed per protocol, including the initiation of an 8% dextrose solution + 2% amino-acid solution at total fluids of 150 ml/kg/d by 3 h of age. This solution was subsequently converted to an 8% dextrose solution + 1/4 normal saline + 2% amino acids by 24 h of age.

Plasma Metabolomics

A total of 49 samples were collected from six primates. Although nine timed samples per animal (54 samples total) were intended, some samples were unable to be processed due to inadequate sample volume or technical collection difficulties. Each sample was run in triplicate, resulting in 147 GC × GC–TOFMS chromatograms. For the discovery stage of the study, 60 chromatograms from primates P1–3 were analyzed using the signal ratio method. A total of 100 metabolites were initially identified that exhibited a (potentially) high degree of change between these time points. Metabolites with a relative standard deviation >30% between replicates were deemed unreliable due to the inability of the instrument to precisely capture those metabolites and hence were excluded from subsequent inquiry. In total, 31 metabolites were excluded on this basis. The complete list of identified metabolites measured with good precision by the instrument with their respective National Institute of Standards and Technology match values (n = 69) is provided in Supplementary Table S1 online in order of their retention time on the first column of the GC × GC separation.

The remaining 69 metabolites were quantified by parallel factor analysis (PARAFAC), generating a list of metabolites that exhibited a concentration change over time. Metabolite concentrations are reported by m/z signal intensity, which is not immediately translatable to clinical serum levels. However, relative changes in metabolite concentration over time are directly provided, and if of interest, absolute quantification can be obtained using metabolite standards. Applying the mixed-model ANOVA to the samples yielded a level of significance of $P < 0.05$ in all metabolites except for glucose and one minor peak of propanoic acid. Subsequent *post hoc* testing with the Dunnett's test demonstrated significant changes in 23 metabolite concentration levels when comparing each time point to the initial cord blood sample (time point: 0 min). The complete list of metabolites with significant change over

time following birth is provided in Supplementary Table S2 online. The *m*/*z* signal intensity is normalized to the total ion current (TIC) in the table.

Table 2 presents the metabolites that significantly changed over time, as identified by the signals ratio method, and divided into metabolite category. Note that the metabolites annotated ([a]) are considered to have a tentative identification, as they were only identified using mass spectral matching to an external library. The metabolites are divided into categories including signaling pathway intermediates, glucose metabolism intermediates, carbohydrates, amino acids, and an assortment of other metabolites. Figure 1 is a heat map illustrating the change in metabolite concentration as it relates to the baseline cord blood for the metabolites listed in Table 2. Metabolites that are upregulated as compared with time point 0 min are designated in Figure 1 with a change in color along the red spectrum, whereas metabolites that decrease have a change in color along the blue spectrum. Some metabolites show a steady increase in concentration (i.e., malic acid, fumaric acid) whereas others show an acute decrease in concentration (i.e., lactic acid).

Four intermediates from the tricarboxylic acid (TCA) cycle (α-ketoglutaric acid, fumaric acid, malic acid, and succinyl-CoA) showed a significant change over time. Individual values from each animal are plotted in Figure 2. Although all four metabolites steadily increase over the course of the first 3 days of age, with the most rapid rate of rise early in the time course, there is considerable interanimal variability.

Two intermediates of signaling pathways were identified: glutamic acid and *myo*-inositol. Figure 3 shows the change of these metabolites for each animal. The concentration of glutamic acid peaks at 6 h of age (Figure 3a); the concentration peak for *myo*-inositol is at 24 h of age (Figure 3b). Other metabolites of interest are lactic acid and its derivatives. After the immediate rise in lactic acid concentration at 5 min of age, the level decreases significantly by 1 h of age. This pattern is opposite of the intermediates found within the TCA cycle. Three metabolites were identified in the primates' blood that represent maternal nutritional components that are not discussed in Table 2 (see Supplementary Table S2 online); each metabolite shows evidence of postnatal clearance by the primate.

DISCUSSION

The fetal-to-neonatal transition is complex, and little data exist that demonstrate the body's response to this process. To our knowledge, this is the first report of the metabolic response to birth and the subsequent transition to extrauterine life. Using validated data analysis tools (18,20,21,25,26), we were able to generate a biochemical profile to describe this transition as it relates to a number of different metabolic cycles and other biochemical intermediates.

The TCA cycle had the most intermediates represented in the biochemical profile. Four intermediates, α-ketoglutaric acid, fumaric acid, malic acid, and succinyl-CoA, were identified with significant changes over the time period. The TCA cycle is crucial in aerobic metabolism, with its intermediates dependent on oxygen and the electron transport chain in the mitochondrial membrane to regenerate nicotinamide adenine dinucleotide and flavin adenine dinucleotide to continue its pathway. Studies have demonstrated that there is an

acute oxidative stress that occurs at birth due to the rapid change in oxygen exposure (5,27). Recent analysis of transcription factors in cord blood of human fetuses revealed a large representation of mitochondrial respiratory chain genes associated with oxidative stress, suggesting that the fetus prepares for this difficult transition with an intricate redox transcriptome (6). Our study adds to the growing body of data indicating there is a molecular transition occurring as the body is exposed to oxygen and can utilize more of it. As Figure 2 demonstrates, all four intermediates slowly increase in concentration over the course of the first 3 days of age, some more directly than others. We speculate that this steady elevation of key intermediates represents the body transition to more aerobic metabolism and demonstrates an ability to utilize the reduction–oxidation pathways of the electron transport chain. Of note, lactic acid decreases rapidly as the TCA-cycle intermediates increase. This may also reflect the body's transition from more anaerobic metabolism with less oxygen available to predominantly aerobic metabolism utilizing the TCA cycle. In our previous study on the discovery of biomarkers of perinatal asphyxia (24), two intermediates of the TCA cycle were isolated: succinic acid and malic acid. In that study, these two intermediates showed dramatic elevation following birth and asphyxia, which was thought to be a result of an interruption of the redox reaction with nicotinamide adenine dinucleotide/flavin adenine dinucleotide due to the hypoxia insult. Our current study does not demonstrate the same pattern of elevation of each metabolite concentration, suggesting that the slow elevation of TCA-cycle intermediates as a result of the birth transition is a different process than the acute elevation of TCA-cycle intermediates that are affected by asphyxia.

Two metabolites were identified that are associated with signaling pathways: *myo*-inositol and glutamic acid. Both metabolites are involved in a number of different biochemical pathways throughout the body. *Myo*-inositol is a precursor for inositol phospholipids, which when cleaved generate the common second messengers inositol 1,4,5-trisphosphate and diacylglycerol (28). These second messengers are important in a variety of cellular functions including intracellular calcium homeostasis (29), gene expression (30,31), and fat metabolism (32). Glutamic acid is a nonessential amino acid that is involved in many metabolic pathways and is also a crucial central nervous system signaling molecule. In cellular metabolism, glutamic acid is a part of the malate–aspartate shuttle, central in the redox reactions of aerobic metabolism by mobilizing nicotinamide adenine dinucleotide from the cytosol to the mitochondria. Glutamic acid is also involved in the urea cycle, allowing the removal of ammonia and urea from the body. As a signaling molecule, glutamic acid is the leading excitatory neurotransmitter in the central nervous system, associated with memory and learning (33). In this study, we found that concentrations of both signaling metabolites changed over the first 3 d of age (Figure 3). *Myo*-inositol peaked at 24 h of age and glutamic acid had an initial peak at 6 h with a secondary lesser peak at 24 h. Of note, glutamic acid was also found to have significant elevation following perinatal asphyxia in our previous report (24). In this study, a dramatic elevation of glutamic acid was not seen immediately following non-asphyxiated birth (at the 5-min time point).

Although the metabolic profile of the perinatal transition generated multiple analytes that change over time, there may be some metabolites that were not able to be identified using GC × GC–TOFMS, such as metabolites that are larger than trisaccharides (34). Despite the

limitations of the instrumental platform (35), numerous studies have demonstrated that GC × GC–TOFMS has the ability to capture large amounts of data with high resolution and accuracy (18,21,25), and no single instrumentation can currently monitor the entire metabolome. In addition, to take the reported information to the clinical arena, the PARAFAC quantification would need to be applied with calibration standards of the derivatized metabolites. Although this was not necessary to achieve the desired goals of this study, absolute quantification could be applied to convert the PARAFAC signal to specific serum levels. More translational studies are needed to connect the information from this study to laboratory serum levels for direct comparison. The number of primates studied is the final limitation to this investigation, having only three nonhuman primates available for the discovery phase and six subjects for relative quantification. Although these low numbers may have led to an incomplete capture of the metabolome of the perinatal transition due to biological variability, we are confident that this study was able to encapsulate a solid foundation for further understanding the biochemical response to birth.

Conclusion

Metabolomic analysis of the transition of a nonhuman primate from an intrauterine to extrauterine environment demonstrates a complex framework of biochemical processes. The novelty of these data adds significantly to the medical literature. First, it supports the importance of the redox balance that has been previously investigated on molecular and genomic levels. More important, because little has been reported on the incremental changes of metabolite concentrations following birth, this study provides foundational information related to the metabolic pattern of perinatal transition. With each metabolite identified, we have a better understanding of the biochemical changes that occur. This profile has the potential to be used in future studies as a baseline normal pattern for metabolites as a function of time. In addition, as future studies are implemented, this metabolomic birth transition profile may aid as a stepping stone for further understanding of pathophysiology and target therapy within the field of perinatology.

METHODS

The Animal Care and Use Committee at the University of Washington, in accordance with US National Institutes of Health guidelines, approved all the experimental protocols.

Primate Delivery Protocol

Time pregnant *Macaca nemestrina* were anesthetized for delivery by hysterotomy at ~170 days (5 ± 2 days before term; $n = 6$). Cord blood was obtained by venipuncture before delivery (36). A 2.5 French umbilical arterial catheter (Vygon, Montgomeryville, PA) was then placed into the ascending aorta via the umbilical cord (37). Following delivery, the primates were stabilized by a team of neonatologists using standardized neonatal resuscitation principles. Apgar scores, vital signs, and serial laboratory parameters were collected. Up to nine timed samples were obtained for each primate: baseline cord blood (time point 0 min) and at 5 min, 1, 3, 6, 12, 24, 48, and 72 h after birth. Samples were collected into heparinized containers, centrifuged at 4 °C, and plasma (200 μl) removed, snap-frozen in liquid nitrogen and stored at −80 °C until metabolite extraction.

Metabolite Extraction, Derivatization, and Instrumentation

Extraction of the metabolites from the plasma was performed using an 8:1 methanol:water solution (by volume), as previously reported (24). Briefly, metabolites were extracted with 2 min of probe sonication, incubated briefly on ice, then centrifuged at 15,000*g* for 10 min to remove cellular debris. Aliquots (200 μl) of the supernatant were transferred to a GC vial and then evaporated to dryness. Derivatization using methoximation and trimethylsilylation was performed on sample extracts to improve thermal stability and volatility of the metabolites for GC-based analysis. Sample volumes (1 μl) were injected in triplicate to GC × GC–TOFMS (LECO, St Joseph, MI). The first column, 20 m × 250 μm internal diameter × 0.5 μm Rtx-5MS (Restek, Bellefonte, PA), separated metabolites primarily by volatility. The second column, 2 m × 180 μm internal diameter × 0.2 μm Rtx-200MS (Restek), separated metabolites primarily based on polarity. Effluent from the second column was detected by the TOFMS where the mass fragment ions generated via electron-impact ionization were collected from mass-to-charge ratio (*m*/*z)* 40–600. Data were collected with the LECO ChromaTOF software, v 3.32 (LECO).

Data Analysis

The signal ratio method (25) was used to identify metabolites with potentially significant differences between the GC × GC–TOFMS chromatograms of samples from the first three primates (P1–3). These samples were processed together and used for metabolite discovery. Samples from subsequent primates were processed later, thus had slight retention-time shifts and were not included in the discovery stage. Metabolites from P1–3 that showed potential differences over time were identified by retention time and mass spectral matching to an in-house library of derivatized metabolite standards, which were processed and categorized using the same instrumentation. Metabolites that were not identified by the in-house library were tentatively identified using external libraries, including the National Institute of Standards and Technology library and the Kyoto Encyclopedia of Genes and Genomes database. Quantification of identified metabolites was performed using PARAFAC, an internally derived mathematical deconvolution algorithm that provides the *m*/*z* signal intensity volume under the curve of each metabolite peak (20). Following the signal ratio method discovery step, the identified metabolites from all six primates were quantified using PARAFAC. Precision of the instrument was determined by calculating the relative standard deviation between injection replicates of each metabolite. To ensure that the changes in the identified metabolites were not due to technical sample variation (e.g., variation in the sample volume injected into the instrument), the TIC was calculated for each sample replicate, and used as the internal standard. The TIC is a measure of the absolute amount of signal detected within the complete injection by the GC × GC–TOFMS instrument and can be used as an internal standard. The TIC can be used as an internal standard by dividing each individual metabolite signal in a given injection by the TIC for the corresponding injection, thus correcting for slight variations within the injection volumes or instrument detection (19).

To evaluate changes in metabolites over time, mixed-model ANOVA was performed on each metabolite individually to include all repeated measures from animals with missing values as sampling was not complete for all animals. The SPSS linear mixed modeling

procedure used: time as a factor, fixed model, diagonal covariance, type 3 sum of squares, 100 iterations, and absolute convergence. For each metabolite with a P value <0.05 with mixed-model ANOVA, *post hoc* testing was performed using Dunnett's test, comparing each sample time point to the baseline cord blood samples. Significance for the Dunnett's test was $P < 0.05$.

Supplementary Material

Refer to Web version on PubMed Central for supplementary material.

Acknowledgments

We thank the infant primate lab staff for all their help with the care of these animals.

STATEMENT OF FINANCIAL SUPPORT

This study was supported by an Institute of Translational Health Sciences Pilot award, National Institutes of Health grant R01-HD-52820-01, and an American Recovery and Reinvestment Act supplement to R01-HD-52820-01 and P30 HD02274 through the Washington Regional Primate Research Center and the National Institute of Child Health and Human Development.

References

1. Blackburn S. Placental, fetal, and transitional circulation revisited. J Perinat Neonatal Nurs. 2006; 20:290–4. [PubMed: 17310669]
2. Askin DF. Fetal-to-neonatal transition–what is normal and what is not? Neonatal Netw. 2009; 28:e33–40. [PubMed: 19451072]
3. Tucker A, Weir EK, Grover RF, Reeves JT. Oxygen-tension-dependent pulmonary vascular responses to vasoactive agents. Can J Physiol Pharmacol. 1977; 55:251–7. [PubMed: 871957]
4. Jain L, Eaton DC. Physiology of fetal lung fluid clearance and the effect of labor. Semin Perinatol. 2006; 30:34–43. [PubMed: 16549212]
5. Friel JK, Friesen RW, Harding SV, Roberts LJ. Evidence of oxidative stress in full-term healthy infants. Pediatr Res. 2004; 56:878–82. [PubMed: 15470194]
6. Maron JL, Johnson KL, Parkin C, Iyer L, Davis JM, Bianchi DW. Cord blood genomic analysis highlights the role of redox balance. Free Radic Biol Med. 2010; 49:992–6. [PubMed: 20566327]
7. Mellor DJ, Pearson RA. Some changes in the composition of blood during the first 24 hours after birth in normal and growth retarded lambs. Ann Rech Vet. 1977; 8:460–7. [PubMed: 615517]
8. Atzori L, Antonucci R, Barberini L, Griffin JL, Fanos V. Metabolomics: a new tool for the neonatologist. J Matern Fetal Neonatal Med. 2009; 22(Suppl 3):50–3. [PubMed: 19701858]
9. Antonucci R, Atzori L, Barberini L, Fanos V. Metabolomics: the "new clinical chemistry" for personalized neonatal medicine. Minerva Pediatr. 2010; 62:145–8. [PubMed: 21089734]
10. Ellis DI, Dunn WB, Griffin JL, Allwood JW, Goodacre R. Metabolic fingerprinting as a diagnostic tool. Pharmacogenomics. 2007; 8:1243–66. [PubMed: 17924839]
11. Bictash M, Ebbels TM, Chan Q, et al. Opening up the "Black Box": metabolic phenotyping and metabolome-wide association studies in epidemiology. J Clin Epidemiol. 2010; 63:970–9. [PubMed: 20056386]
12. Oliver SG, Winson MK, Kell DB, Baganz F. Systematic functional analysis of the yeast genome. Trends Biotechnol. 1998; 16:373–8. [PubMed: 9744112]
13. Bligny R, Douce R. NMR and plant metabolism. Curr Opin Plant Biol. 2001; 4:191–6. [PubMed: 11312128]
14. Bundy JG, Spurgeon DJ, Svendsen C, et al. Earthworm species of the genus *Eisenia* can be phenotypically differentiated by metabolic profiling. FEBS Lett. 2002; 521:115–20. [PubMed: 12067738]

15. García A, Barbas C, Aguilar R, Castro M. Capillary electrophoresis for rapid profiling of organic acidurias. Clin Chem. 1998; 44:1905–11. [PubMed: 9732975]
16. Barsch A, Patschkowski T, Niehaus K. Comprehensive metabolite profiling of *Sinorhizobium meliloti* using gas chromatography-mass spectrometry. Funct Integr Genomics. 2004; 4:219–30. [PubMed: 15372312]
17. Tetsuo M, Zhang C, Matsumoto H, Matsumoto I. Gas chromatographic-mass spectrometric analysis of urinary sugar and sugar alcohols during pregnancy. J Chromatogr B Biomed Sci Appl. 1999; 731:111–20. [PubMed: 10491996]
18. Pierce KM, Hoggard JC, Hope JL, et al. Fisher ratio method applied to third-order separation data to identify significant chemical components of metabolite extracts. Anal Chem. 2006; 78:5068–75. [PubMed: 16841931]
19. Mohler RE, Dombek KM, Hoggard JC, Young ET, Synovec RE. Comprehensive two-dimensional gas chromatography time-of-flight mass spectrometry analysis of metabolites in fermenting and respiring yeast cells. Anal Chem. 2006; 78:2700–9. [PubMed: 16615782]
20. Hoggard JC, Synovec RE. Parallel factor analysis (PARAFAC) of target analytes in GC × GC-TOFMS data: automated selection of a model with an appropriate number of factors. Anal Chem. 2007; 79:1611–9. [PubMed: 17297963]
21. Mohler RE, Dombek KM, Hoggard JC, Pierce KM, Young ET, Synovec RE. Comprehensive analysis of yeast metabolite GC × GC-TOFMS data: combining discovery-mode and deconvolution chemometric software. Analyst. 2007; 132:756–67. [PubMed: 17646875]
22. Pierce KM, Hoggard JC, Mohler RE, Synovec RE. Recent advancements in comprehensive two-dimensional separations with chemometrics. J Chromatogr A. 2008; 1184:341–52. [PubMed: 17697686]
23. Pierce KM, Hope JL, Hoggard JC, Synovec RE. A principal component analysis based method to discover chemical differences in comprehensive two-dimensional gas chromatography with time-of-flight mass spectrometry (GC×GC-TOFMS) separations of metabolites in plant samples. Talanta. 2006; 70:797–804. [PubMed: 18970842]
24. Beckstrom AC, Humston EM, Snyder LR, Synovec RE, Juul SE. Application of comprehensive two-dimensional gas chromatography with time-of-flight mass spectrometry method to identify potential biomarkers of perinatal asphyxia in a non-human primate model. J Chromatogr A. 2011; 1218:1899–1906. [PubMed: 21353677]
25. Mohler RE, Tu BP, Dombek KM, Hoggard JC, Young ET, Synovec RE. Identification and evaluation of cycling yeast metabolites in two-dimensional comprehensive gas chromatography-time-of-flight-mass spectrometry data. J Chromatogr A. 2008; 1186:401–11. [PubMed: 18001745]
26. Humston EM, Dombek KM, Hoggard JC, Young ET, Synovec RE. Time-dependent profiling of metabolites from *Snf1* mutant and wild type yeast cells. Anal Chem. 2008; 80:8002–11. [PubMed: 18826242]
27. Saugstad OD. Update on oxygen radical disease in neonatology. Curr Opin Obstet Gynecol. 2001; 13:147–53. [PubMed: 11315869]
28. Downes CP, Carter AN. Inositol lipids and phosphates. Curr Opin Cell Biol. 1990; 2:185–91. [PubMed: 2163656]
29. Streb H, Irvine RF, Berridge MJ, Schulz I. Release of Ca^{2+} from a nonmitochondrial intracellular store in pancreatic acinar cells by inositol-1,4,5-trisphosphate. Nature. 1983; 306:67–9. [PubMed: 6605482]
30. Shen X, Xiao H, Ranallo R, Wu WH, Wu C. Modulation of ATP-dependent chromatin-remodeling complexes by inositol polyphosphates. Science. 2003; 299:112–4. [PubMed: 12434013]
31. Steger DJ, Haswell ES, Miller AL, Wente SR, O'Shea EK. Regulation of chromatin remodeling by inositol polyphosphates. Science. 2003; 299:114–6. [PubMed: 12434012]
32. Rapiejko PJ, Northup JK, Evans T, Brown JE, Malbon CC. G-proteins of fat-cells. Role in hormonal regulation of intracellular inositol 1,4,5-trisphosphate. Biochem J. 1986; 240:35–40. [PubMed: 3103610]
33. McEntee WJ, Crook TH. Glutamate: its role in learning, memory, and the aging brain. Psychopharmacology (Berl). 1993; 111:391–401. [PubMed: 7870979]

34. Weckwerth W, Fiehn O. Can we discover novel pathways using metabolomic analysis? Curr Opin Biotechnol. 2002; 13:156–60. [PubMed: 11950569]

35. Dunn WB, Bailey NJ, Johnson HE. Measuring the metabolome: current analytical technologies. Analyst. 2005; 130:606–25. [PubMed: 15852128]

36. Jacobson Misbe EN, Richards TL, McPherson RJ, Burbacher TM, Juul SE. Perinatal asphyxia in a nonhuman primate model. Dev Neurosci. 2011; 33:210–21. [PubMed: 21659720]

37. Juul SE, Aylward E, Richards T, McPherson RJ, Kuratani J, Burbacher TM. Prenatal cord clamping in newborn *Macaca nemestrina*: a model of perinatal asphyxia. Dev Neurosci. 2007; 29:311–20. [PubMed: 17762199]

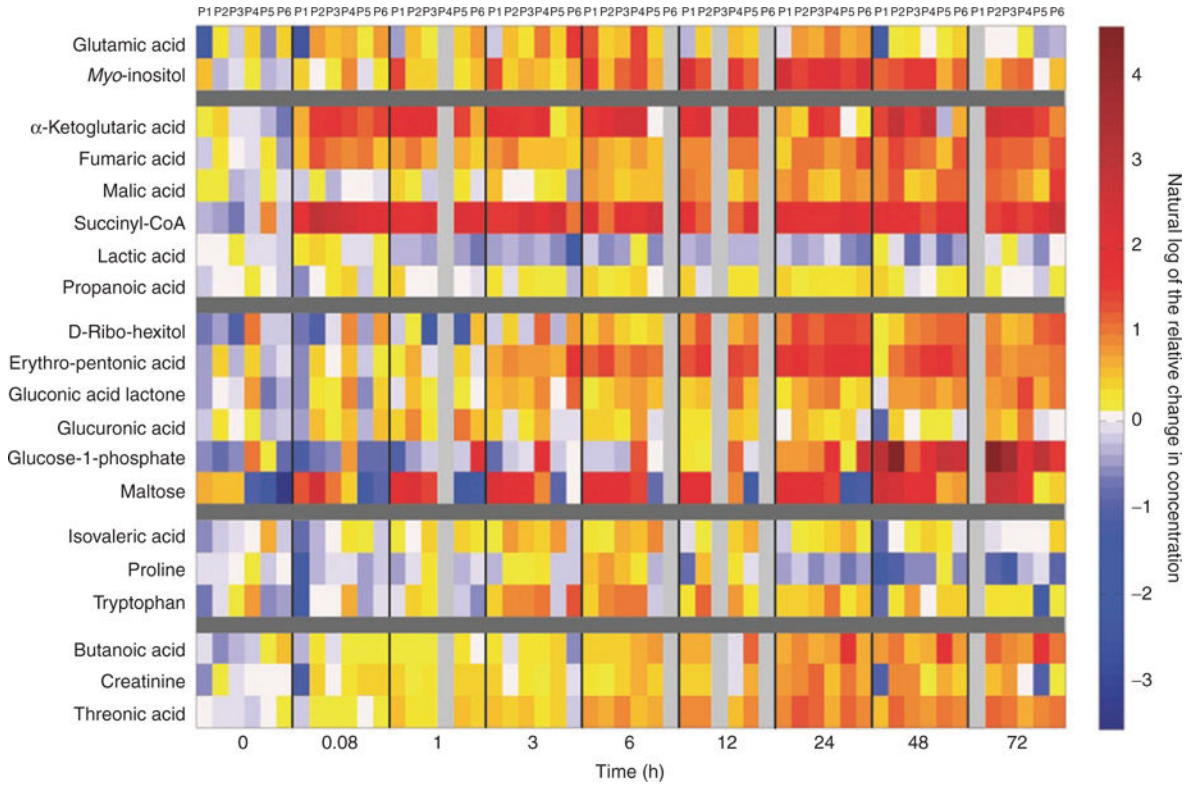

Figure 1.

Heat map demonstrating the change in concentration of metabolites associated with the birth transition relative to time point 0. The 20 identified metabolites are listed on the *y*-axis, divided into metabolite categories from Table 2. The individual time points 0–72 h are listed on the *x*-axis, additionally subdivided by individual primate (P1–6). Each square represents the metabolite concentration of one analyte for one primate at one time point. Each value is the natural log of the concentration change relative to time point 0 determined by dividing the respective value by the mean of time point zero. Time points with colors along the red spectrum are >0 (the natural log of 1), which translates into an increased *m*/*z* signal intensity and metabolite concentration as compared with time point 0. Time points with colors along the blue spectrum are <0 (the natural log of 1), demonstrating a decrease in metabolite concentration as compared with time point 0.

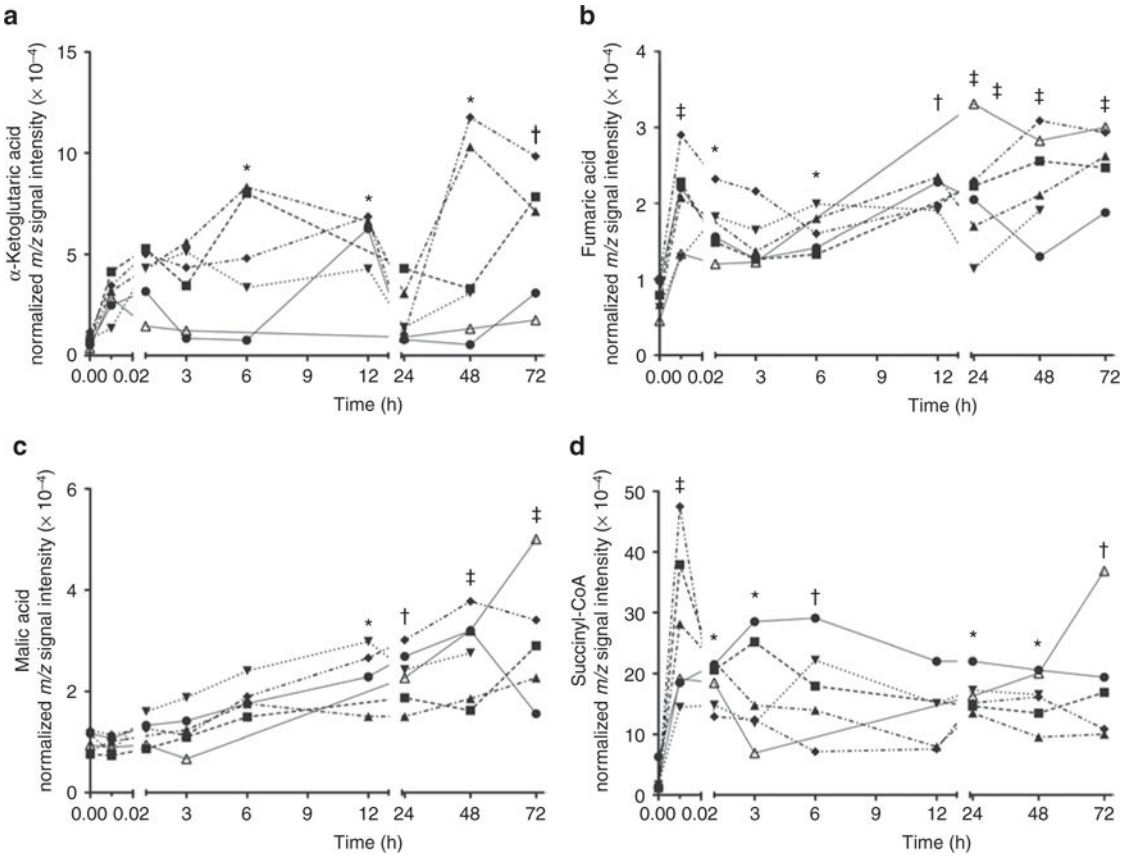

Figure 2.

Tricarboxylic acid (TCA)-cycle intermediates and the change in their normalized *m*/*z* signal intensity over the first 72 h of age. (**a**) α-Ketoglutaric acid, (**b**) fumaric acid, (**c**) malic acid, and (**d**) succinyl-CoA. Each individual line represents the change in the specified metabolite over time for each primate (P1–6) plotted independently. Each metabolite slowly increases over the time course demonstrated on the *x*-axis. After mixed-model ANOVA, *post hoc* Dunnett's tests comparing individual time points to time point zero are demonstrated: $^{*}P < 0.05$; $^{\dagger}P < 0.01$; $^{\ddagger}P < 0.001$.

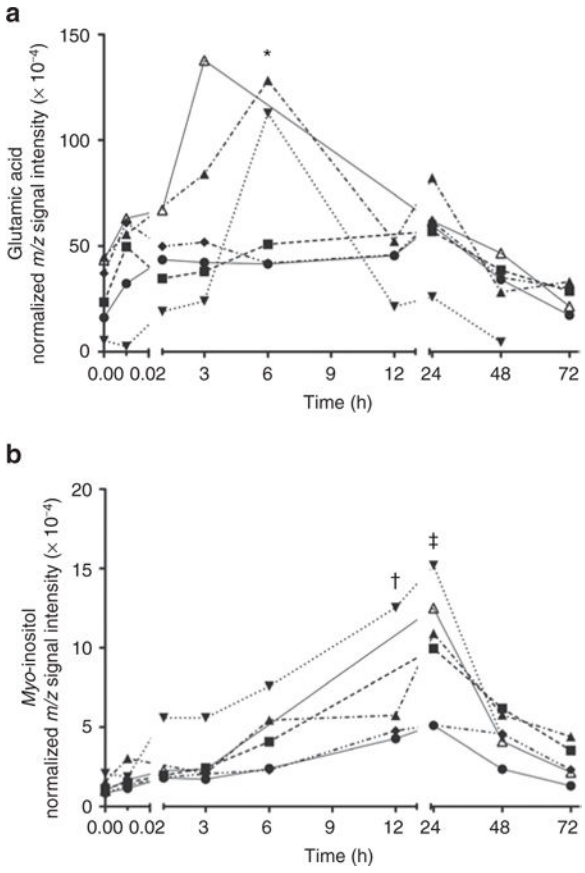

Figure 3.

Signaling pathway intermediates and the change in their normalized *m*/*z* signal intensity over the first 72 h of age. (**a**) Glutamic acid slowly increases with an analyte peak at 6 h of age. (**b**) *Myo*-inositol peaks at 24 h of age. Each individual line represents the change in the specified metabolite over time for each primate (P1–6) plotted independently. After mixed-model ANOVA, *post hoc* Dunnett's tests comparing individual time points to time point zero are demonstrated: $^{*}P < 0.05$; $^{\dagger}P < 0.01$; $^{\ddagger}P < 0.001$.

Table 1

Primate characteristics (mean ± SD)

Birth weight (g)	543.8 ± 61.9
Sex (male:female)	4:2
Apgar scores	
1 min	4.2 ± 1.1
5 min	5.7 ± 1.8
10 min	7.7 ± 0.8
Vital signs	
Temperature (°C)	36.3 ± 1.2
Heart rate (beats/min)	173 ± 25
Respiratory rate (breaths/min)	84 ± 22
Oxygen saturation (%)	91 ± 6
Blood pressure (mm Hg)[a]	56–142/21–102
Mean arterial pressure (mm Hg)	78 ± 35
Labs at 0 min (cord blood)	
pH	7.21 ± 0.13
PCO_2 (mm Hg)	54.4 ± 15
Base excess	−6.8 ± 4.5
Lactate (mmol/l)	5.8 ± 2.6
Labs at 3 h	
pH	7.36 ± 0.04
PCO_2 (mm Hg)	42.4 ± 6
Base excess	−2.0 ± 1.9
Lactate (mmol/l)	2.0 ± 1.1

PCO_2, partial CO_2.

[a]Range of systolic blood pressure/diastolic blood pressure.

Table 2

Metabolites that significantly change during the birth transition

Metabolic category	Pathway/description
Signaling intermediates	
Glutamic acid	Excitatory neurotransmitter; malate–aspartate shuttle; urea cycle
Myo-inositol	Second messenger system, including intracellular calcium homeostasis, gene expression, fat metabolism
Glucose metabolism	
α-Ketoglutaric acid	TCA cycle; malate–aspartate shuttle
Fumaric acid	TCA cycle; urea cycle
Malic acid	TCA cycle; malate–aspartate shuttle
Succinyl-CoA	TCA cycle; leucine/isoleucine/valine end point of metabolism
Lactic acid	Anaerobic metabolic pathway
Propanoic acid[a]	Derivative of lactic acid; anaerobic metabolic pathway
Carbohydrates and derivatives	
D-Ribo-hexitol[a]	Six-carbon sugar alcohol
Erythro-pentonic acid[a]	Isosaccharinic acid; six-carbon sugar acid
Gluconic acid lactone[a]	Glucose metabolite
Glucuronic acid[a]	Xenobiotic metabolism (glucuronidation in liver); proteoglycan
Glucose-1-phosphate	Gluconeogenesis intermediate; galactose utilization
Maltose	Disaccharide
Amino acids and derivatives	
Isovaleric acid[a]	Isoleucine metabolism
Proline[a]	Ornithine metabolism; derived from glutamic acid
Tryptophan	Essential amino acid; precursor for serotonin and niacin
Miscellaneous	
Butanoic acid[a]	Short-chain fatty acid
Creatinine	Marker for renal function
Threonic acid	Vitamin C metabolism

TCA, tricarboxylic acid.

[a]Tentative identification defined as metabolites that were identified with external libraries (i.e., National Institute of Standards and Technology library) and did not have retention time matching to the in-house library of metabolite standards.